Cherenkov Light Emission in Pure Cherenkov Emitters for Prompt Gamma Imaging

L. Rebolo[ID], C. Trigila[ID], *Associate Member, IEEE*, J. Ellin, P. M. Mendes Correia, A. L. Silva, J. Veloso, S. St. James, E. Roncali[ID], *Senior Member, IEEE*, and G. Ariño-Estrada[ID], *Member, IEEE*

Abstract—Proton range verification (PRV) in proton therapy by means of prompt-gamma detection is a promising but challenging approach. High-count rates, energies ranging between 1 and 7 MeV, and a strong background complicate the detection of such particles. In this work, the Cherenkov light generated by prompt-gammas in the pure Cherenkov emitters thallium bromide, thallium chloride (TlCl) and PbF_2 was studied. Cherenkov light in these crystals can provide a very fast timing signal with the potential to achieve very high-count rates and to discern between prompt-gammas and background signals. Crystals of 1×1 cm^2 and thicknesses of 1, 2, 3, and 4 cm were simulated. Different photodetector (PD) configurations were studied for 2.3, 4.4, and 6.1-MeV prompt-gammas. TlCl achieved the greatest number of detected Cherenkov photons for all energies, detector dimensions, and PD efficiency modeling. For the highest-prompt-gamma energy simulated, TlCl yielded approximately 250 Cherenkov detected photons, using a hypothetical high-performance PD. Results show the crystal blocks of 1 cm × 1 cm × 1 cm have greater prompt-gamma detection efficiency per volume and a comparable average number of detected Cherenkov photons per event.

Index Terms—Cherenkov emitters, Cherenkov light, prompt-gamma imaging (PGI), proton range verification (PRV).

I. INTRODUCTION

Prompt gamma imaging (PGI) is one of the proposed methods for proton range verification (PRV) in proton radiotherapy (PR) [1], [2]. PGI aims to monitor the position of the Bragg Peak in PR using the information provided by prompt-gammas emitted during nuclear de-excitations of target nuclei, predominantly carbon and oxygen [3]. The emission profile of prompt-gammas is strongly correlated with the dose distribution of protons in the target, showing a significantly greater emission in the Bragg peak region, with a few millimeters offset [4].

While prompt-gammas in this application have energies between 1 and 7 MeV [1], [5], the lines at 4.4 and 6.1 MeV attract most interest

This work did not involve human subjects or animals in its research.

L. Rebolo, C. Trigila, J. Ellin, and G. Ariño-Estrada are with the Department of Biomedical Engineering, University of California at Davis, Davis, CA 95616 USA (e-mail: lerebolo@ucdavis.edu; garino@ucdavis.edu).

P. M. Mendes Correia, A. L. Silva, and J. Veloso are with the I3N-Physics Department, University of Aveiro, 3810-193 Aveiro, Portugal.

S. St. James is with the Huntsman Cancer Center, University of Utah, Salt Lake City, UT 84112 USA.

E. Roncali is with the Department of Biomedical Engineering and the Department of Radiology, University of California at Davis, Davis, CA 95616 USA.

Properties		TlBr	TlCl	PbF_2
Density [g/cm^3]		7.5	7.0	7.8
Attenuation length [cm]	2.3 MeV	3.1	3.3	3.0
	4.4 MeV	3.4	3.5	3.2
	6.1 MeV	3.3	3.4	3.1
Refractive index at 550 nm		2.48	2.32	1.78
Cutoff wavelength [nm]		440	380	250

because they have relatively high-cross section compared to the rest and seem to provide a relative enhancement of the discrimination of the distal dose falloff, compared to lower-energy lines [6], [7], [8]. Besides, prompt-gammas are emitted within few picoseconds after nuclear interactions, unlike the decay of other byproducts of the proton beam, such as positron emitters, which otherwise suffer from biological washout and range effects [9], [10], [11]. Nonetheless, very high-count rates, the presence of intense background, and much greater energies compared to other medical imaging modalities in nuclear medicine and radiology, pose unique challenges to the clinical use of PGI [12].

This work focuses in the study of Cherenkov light generated by prompt-gammas in thallium bromide (TlBr), thallium chloride (TlCl) and lead fluoride (PbF_2), which are pure Cherenkov emitters with high-detection efficiency. Table I summarizes their physical properties.

The rate of prompt-gammas in PR for typical beam currents, between a few hundreds of pA to tens of nA, is approximately 10^8 prompt-gammas per second or greater [16], [17]. For relatively big detectors consisting of scintillation crystals, such rates will lead to pile-up effects unless a collimation method is used.

Oppositely to scintillation light, Cherenkov light is emitted entirely within few picoseconds after the interaction of the prompt-gamma in the material, which can enable much greater count rates than scintillation-based detectors. Moreover, the average value of detected Cherenkov photons for 511-keV gamma interactions is between 1 and 3 using TlBr, TlCl [13] and PbF_2 [18] crystals, and therefore it is practically insensitive to this source of background when a moderate hardware threshold is set.

The accurate time-stamp provided by Cherenkov light allows the use of time-of-flight-based gating to reduce the background due to neutron-induced prompt-gammas [19]. PGI using prompt gamma timing (PGT) has been studied with PbF_2 detectors coupled to silicon photomultipliers (SiPMs) [20]. Cherenkov light in TlBr and TlCl were also studied for time-of-flight positron emission tomography (TOF-PET) [13], [21]. Additionally, TlBr Cherenkov Charge Induction gamma detector for 511-keV and 1.275-MeV gamma energies was reported [22], [23]. Despite the efforts to model and understand the emission of Cherenkov light of these and other heavy materials for 511 keV, such as bismuth germanate (BGO) [24], [25], no comprehensive study of the yield
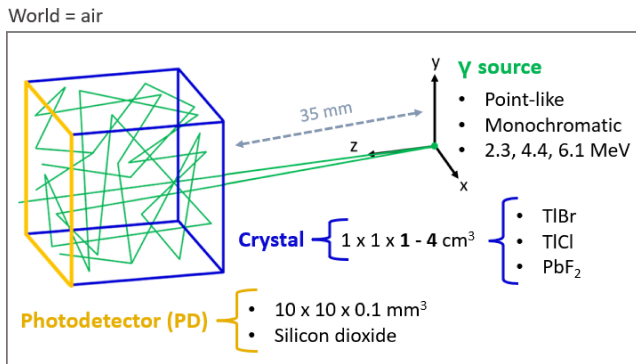
Fig. 1.   Illustration of the simulation setup.

of Cherenkov light, physics interaction process, and effect of detector configuration for prompt-gammas, has been reported to our knowledge.

In this work, the Cherenkov light yield was simulated in TlBr, TlCl, and PbF$_2$ crystals for different detector configurations, prompt-gamma energy lines, and using different photodetectors (PDs).

II. MATERIALS AND METHODS

A. Radiation-Matter Interaction

The toolkit GATE v9.0 (Geant4 10.06.03 and ROOT 6.20) was used to simulate the radiation-matter interactions among prompt-gammas, crystal block and PD.

Crystal blocks of 1×1-cm^2 cross sections with varying thickness between 1 and 4 cm (Fig. 1) were simulated. The PD was modeled as a 0.1-mm thick layer of silicon dioxide attached with optical grease to the back face of the crystal.

A monochromatic gamma source with discrete gamma-lines with 2.3, 4.4, and 6.1 MeV was used to model the prompt-gamma lines from the Bragg Peak. The source was set at 35 mm from the closer face of the crystal, modeled as point-like with isotropic emission. A total of 500 000 gammas were simulated for each scenario. The system was placed in air.

Compton, photoelectric and pair production effects were enabled using the Livermore model. Positron annihilation, multiple scattering and electron ionization, which was modeled with the Standard model, were also enabled.

B. Optical Transport and Detection

The optical transport was modeled with the LUT Davis model [26] and the interface crystal-PD was defined as a polished surface coupled to the PD with optical grease (index of refraction 1.5), assuming 100% transparency for Cherenkov photons with a wavelength longer than 300, 360, and 440 nm for PbF$_2$, TlCl, and TlBr, respectively, and no transmission below that value (Fig. 2).

Three photodetection efficiency (PDE) scenarios were modeled.
1) HPK S14160-3050HS, as used in [13], is a SiPM produced by Hamamatsu Photonics with approximately 75% PDE at 420 nm for an overvoltage of 5 V.
2) FBK NUV-HD, is a SiPM produced by FBK, with approximately 60% at 420 nm for an overvoltage of 3 V.
3) Hypothetical PD with 100% PDE for wavelengths longer than 300 nm and 0% PDE below that value, referred to as "High-PDE PD." This PD modeled the ideal detection efficiency scenario.

The energy deposited (EDEP) was defined for each event as the sum of the energy from all particles emitted by the interactions of the incident gammas within the event.
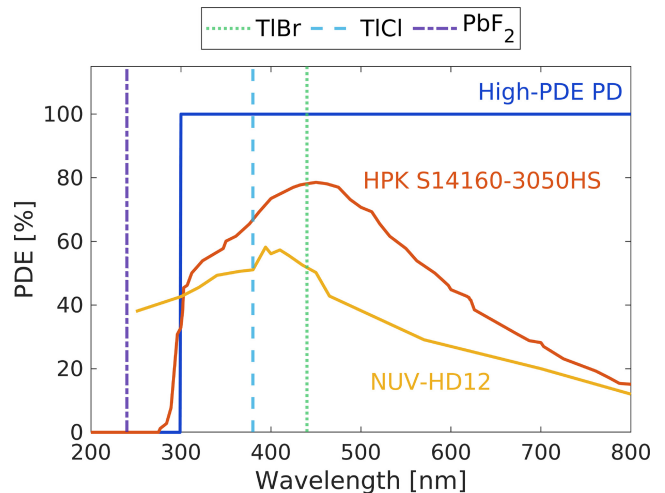

Fig. 2.   Modeled PDE curves used in the PDE scenarios simulated: high-PDE PD (100% PDE >300 nm) (dark blue), HPK S14160-3050HS (orange), and FBK NUV-HD (yellow). The cuttoff wavelength of each material was plotted in different line styles: dotted (TlBr), dashed (TlCl), and dashed-dotted (PbF$_2$).

III. RESULTS

A. Detection Efficiency

Fig. 3 shows the number of prompt-gammas absorbed across materials and thicknesses, for each prompt-gamma energy simulated.

Fig. 4 shows the detected Cherenkov yield for 1-cm thick crystals, for each material and prompt-gamma energy simulated, using High-PDE, HPK S14160-3050HS PDE, and FBK NUV-HD PDE. The NUV-HD was the least efficient PD, achieving the lowest value of detected Cherenkov photons for all materials and energies considered. Among materials, TlCl achieved the greatest value of detected Cherenkov photons for the three PDE scenarios.

B. Interaction Processes and Cherenkov Detection

Fig. 5 shows the event EDEP versus detected Cherenkov photons histogram for 1-cm thick TlCl using 4.4-MeV prompt-gammas. The dataset was sorted according to the interaction process of the parent gamma (gamma originating the event). The EDEP is mostly contributed by the energy of the photoelectrons. The interaction processes and Cherenkov light yield were shown to be strongly associated with energy.

Fig. 6 shows the distributions of detected Cherenkov photons per event in a 1-cm thick TlCl crystal for each prompt-gamma energy simulated. The percentages correspond to the relative contribution of each interaction process to the dataset.

For 4.4 and 6.1 MeV, the distributions consisted of a combination of a plateau for lower-detection values, and a Gaussian shape, predominantly due to pair creation events, at greater values. The 2.3 MeV distribution showed a rather irregular shape, given greater contributions from Compton and Photoelectric events. Photoelectric events occurred the least often but had the highest-detected Cherenkov yield.

As the incident gamma ray energy increases, pair production became the predominant interaction process, as expected. Compton events dominated at 2.3 MeV, at approximately 80%, while pair production events dominated at 6.1 MeV, at approximately 55%.

C. Detected Cherenkov Yield

Fig. 7 shows the results for detected Cherenkov photons in 1 and 4-cm thick TlBr, TlCl, and PbF$_2$ crystals, obtained for each prompt-gamma energy simulated using the HPK S14160-3050HS PDE.
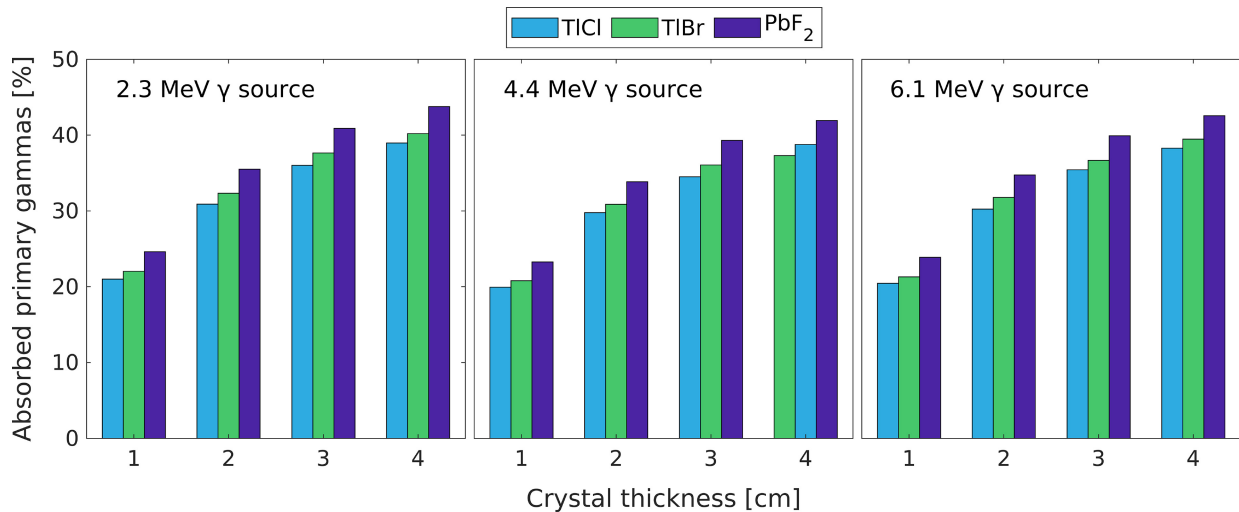
Fig. 3.   Absorbed primary gammas for 1, 2, 3, and 4-cm thick TlBr, TlCl, and PbF$_2$ crystals using 2.3 MeV (left), 4.4 MeV (middle), and 6.1 MeV (right) prompt-gammas. The percentage of absorbed events is defined as the fraction between the number of absorbed primary gammas in the crystal over the total number of gammas crossing the crystal for each scenario.
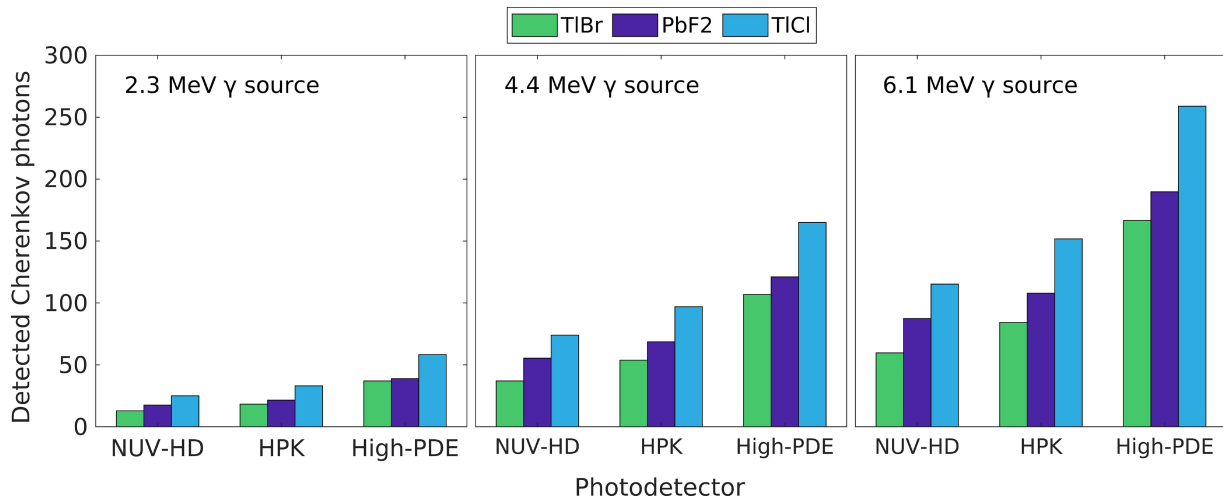

Fig. 4.   Detected Cherenkov yield for 1-cm thick TlBr, TlCl, and PbF$_2$ crystals, using 2.3 (right), 4.4 (middle), and 6.1 (right) MeV prompt-gammas, for different PDEs: high-PDE, HPK S14160-3050HS PDE, and FBK NUV-HD PDE.

For each material, the number of detected Cherenkov photons had minimal variation between thicknesses, whereas the total number of events increased with increasing crystal length. The number of events impacts the height of the distributions and its increase derives from the capacity of thicker crystals to provide greater gamma interaction and, consequently, more generation of secondary particles (such as optical photons). Nonetheless, the mean of the distributions was almost entirely dependent on the prompt-gamma energy, with greater gamma energies leading to greater values of detected Cherenkov photons. A Gaussian fit was used for all energies despite the irregular shape of 2.3-MeV distributions.

TlCl achieved the highest-detection performance for all scenarios out of the three materials. The number of detected Cherenkov photons ranged from 33 photons, at 2.3 MeV, to approximately 150 Cherenkov photons, at 6.1 MeV.

Fig. 8 shows the mean of the fit to the detected Cherenkov photons distributions as a function of the prompt-gamma energy for 1-cm thick crystals using high-PDE PD. In comparison with TlBr and PbF$_2$, results suggest TlCl can resolve each distribution of detected Cherenkov photons for each energy more effectively.

IV. DISCUSSION

Simulations allowed to focus the study on the gamma interactions with the crystal and on the impact of the intrinsic characteristics of each material in the generation and detection of Cherenkov light. Prompt-gamma energy was the main factor affecting the number of detected Cherenkov photons per event. The dominant interaction processes were Compton scattering and pair production at 2.3 and 6.1 MeV, respectively.

The number of detected Cherenkov photons varied with material choice, ranging from approximately 84 Cherenkov photons with TlBr to 152 with TlCl, at 6.1 MeV. While the relative peak position and shape at different energies were comparable across materials, TlCl showed a greater difference among peak positions for each of the energies (Fig. 8). This result suggests an energy threshold based on Cherenkov light could be applied to reject events with lower energies that do not provide meaningful information for PGI.

The PD choice did affect significantly the average number of detected Cherenkov photons per event (Fig. 4). Despite the lower-cut-off wavelength of PbF$_2$, the average number of detected Cherenkov photons in TlCl was greater, even with the high-PDE PD. These
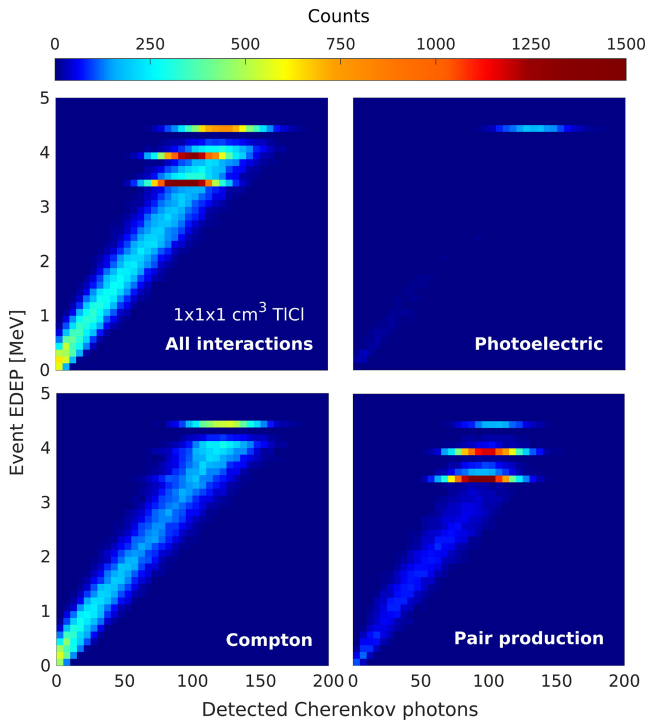
Fig. 5.   EDEP per event versus detected Cherenkov photons for $1\times1\times1$-cm^3 TlCl using 4.4-MeV prompt-gammas. The dataset was sorted according to the interaction process of the parent gamma (gamma originating the event).
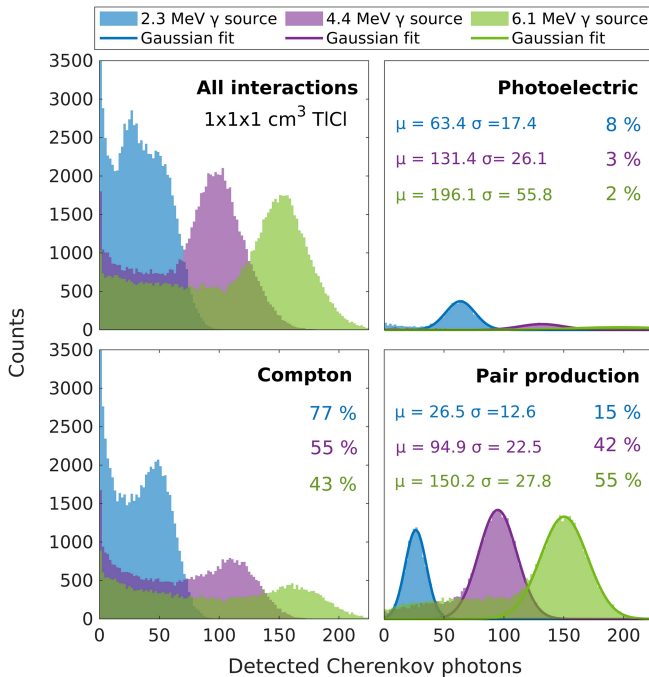

Fig. 6.   Detected Cherenkov photons in $1\times1\times1$-cm^3 TlCl crystal using 2.3 MeV (blue), 4.4 MeV (purple), and 6.1-MeV (green) prompt-gammas and HPK S14160-3050HS PDE. The dataset was sorted according to the interaction process of the parent gamma (gamma originating the event).

results are likely due to the balance between index of refraction and cutoff wavelength of TlCl.

The number of detected Cherenkov photons per event did not seem to depend on the crystal length. Only the total number of absorbed prompt-gammas was impacted by varying thickness, given the greater active volume of longer crystals.
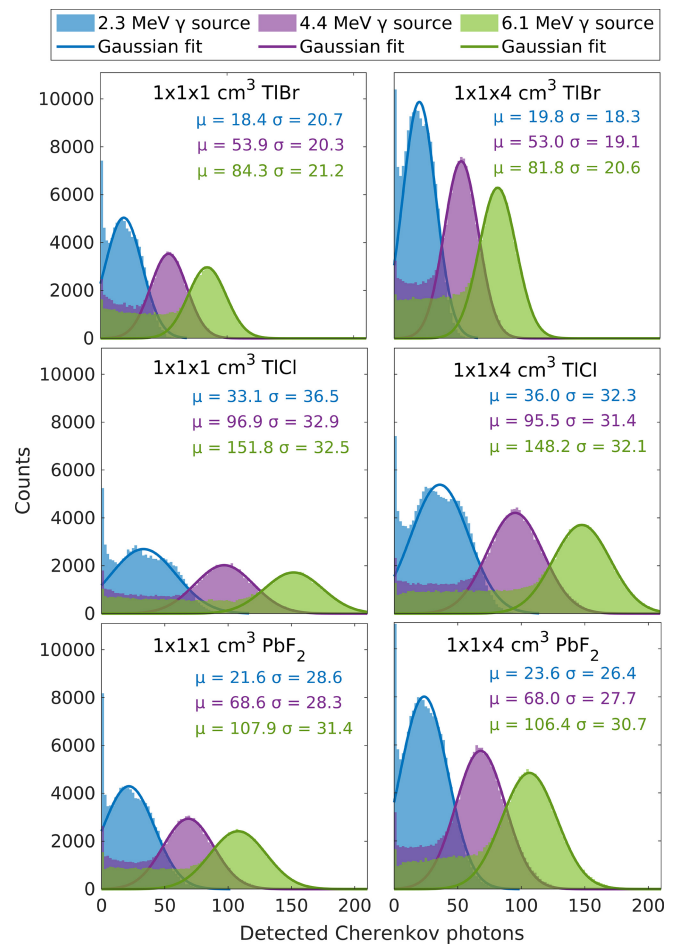

Fig. 7.   Detected Cherenkov photons (μ) in 1 and 4-cm thick TlBr (top), TlCl (middle), and PbF_2 (bottom) crystals, using HPK S14160-3050HS PDE, for all simulated energies. μ and σ are the Gaussian fit parameters.

PbF_2 was the material with more absorbed promt-gammas, although followed very closely by both TlBr and TlCl.

This study is a simplification of the real scenario, where these and other prompt-gamma lines overlap together with other particle emissions. The 2.3-MeV line is representative of the lower-prompt-gamma lines involved with the process, which are poorer signatures of the Bragg Peak position, as well as the 2.2-MeV gamma line created by the deuterium disintegration.

The Cherenkov light yields predicted in this study are less intense than typical scintillation light. For example, for the 4.4 and 6.1-MeV prompt-gammas, the Cherenkov light detected is, approximately between 5% and 10% of the scintillation light detected in a typical BGO crystal in a 511-keV deposition. Nevertheless, the inherent rejection of 511-keV gammas and fast decay time, give Cherenkov light an intrinsically high-signal-to-noise ratio and a potential for very high-count rates.

Different PGI techniques will benefit from specific detector requirements, thus imposing different criteria for material choice. PGT requires excellent timing resolution, whereas in Compton cameras the energy resolution and detector segmentation are crucial. The materials studied can be considered as good candidates for PGT given their potential for timing performance. TlBr showed energy resolutions between 1-2% at 662 keV with pixelated detectors [27], thus hinting the capacity to add accurate energy resolution to the timing information provided by the Cherenkov light. The expected sensitivity of a system using Cherenkov light with either of the
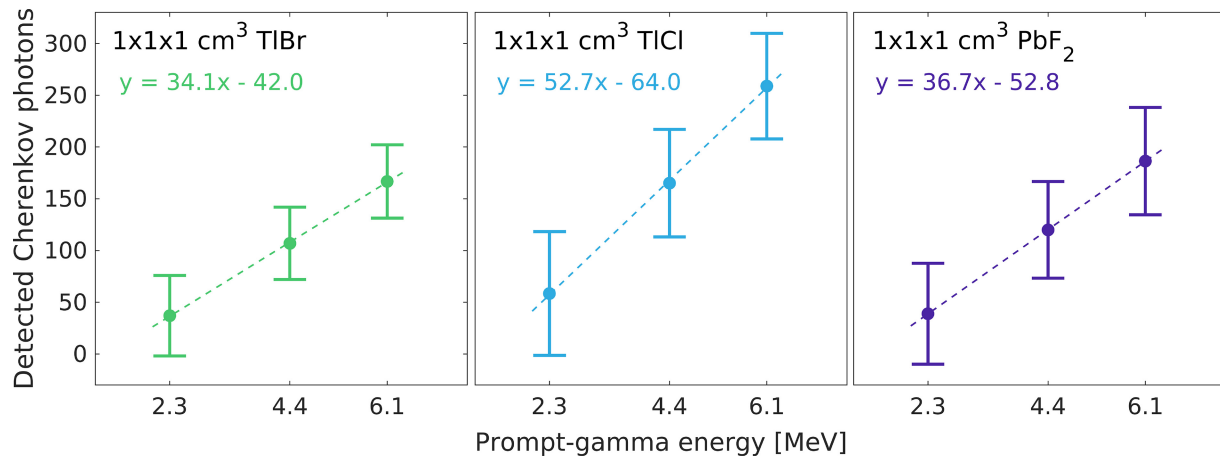
Fig. 8. Detected Cherenkov photons (μ) as a function of prompt-gamma energy, using high-PDE PD, for 1-cm thick TlBr (left), TlCl (middle), and PbF$_2$ (right) crystals. The error bars correspond to the standard deviation of the respective Gaussian fits. Linear fits represented with dashed lines. Linear fit coefficients included as insets.

studied materials is beyond the scope of the current work because it is heavily dependent on the geometry of the envisioned device.

V. CONCLUSION

The generation and detection of Cherenkov light were studied in pure Cherenkov emitters, using different detector configurations and photodetection efficiencies. This study showed that, at the MeV energy range, Cherenkov light detection yield is strong enough to be used as practical signal for PRV in several Cherenkov emitters and for different gamma lines. Cherenkov light seems to be a very effective signal to discriminate prompt-gammas originated in the BP from other background signals (contrast to noise) and improve the confidence of PR treatments.

Simulations show a strong linear relation between the detected Cherenkov yield and the EDEP by the prompt-gamma. This information could be leveraged in the design of future Cherenkov enabled PGI systems, which can benefit from specific interaction processes and energy cuts.

ACKNOWLEDGMENT

REFERENCES

[1] A. Wrońska et al., "Prompt gamma imaging in proton therapy— Status, challenges and developments," in *Proc. J. Phys. Conf. Ser.*, 2020, p. 012021. [Online]. Available: https://dx.doi.org/10.1088/1742-6596/1561/1/012021

[2] Y. Xie et al., "Prompt gamma imaging for in vivo range verification of pencil beam scanning proton therapy," *Int. J. Radiat. Oncol. Biol. Phys.*, vol. 99, no. 1, pp. 210–218, Sep. 2017. [Online]. Available: https://www.sciencedirect.com/science/article/pii/S0360301617308489

[3] F. Hueso-González et al., "Compton camera and prompt gamma ray timing: Two methods for in vivo range assessment in proton therapy," *Front. Oncol.*, vol. 6, p. 80, Apr. 2016. [Online]. Available: https://www.frontiersin.org/articles/10.3389/fonc.2016.00080

[4] J. C. Polf, D. Mackin, E. Lee, S. Avery, and S. Beddar, "Detecting prompt gamma emission during proton therapy: The effects of detector size and distance from the patient," *Phys. Med. Biol.*, vol. 59, no. 9, pp. 2325–2340, Apr. 2014. [Online]. Available: https://dx.doi.org/10.1088/0031-9155/59/9/2325

[5] K. T. Lesko et al., "Measurements of cross sections relevant to γ-ray line astronomy," *Phys. Rev. C*, vol. 37, pp. 1808–1817, May 1988. [Online]. Available: https://link.aps.org/doi/10.1103/PhysRevC.37.1808

[6] J. M. Verburg and J. Seco, "Proton range verification through prompt gamma-ray spectroscopy," *Phys. Med. Biol.*, vol. 59, no. 23, pp. 7089–7106, Nov. 2014. [Online]. Available: https://dx.doi.org/10.1088/0031-9155/59/23/7089

[7] C. H. Min, H. R. Lee, C. H. Kim, and S. B. Lee, "Development of array-type prompt gamma measurement system for in vivo range verification in proton therapy," *Med. Phys.*, vol. 39, no. 4, pp. 2100–2107, Apr. 2012. [Online]. Available: https://aapm.onlinelibrary.wiley.com/doi/abs/10.1118/1.3694098

[8] S. Kurosawa et al., "Prompt gamma detection for range verification in proton therapy," *Curr. Appl. Phys.*, vol. 12, no. 2, pp. 364–368, Mar. 2012. [Online]. Available: https://www.sciencedirect.com/science/article/pii/S1567173911004123

[9] M. Hosobuchi, J. Kataoka, F. Nishi, R. Tanaka, and T. Inaniwa, "Demonstrative measurement of proton-nuclear reaction by deconvolving the prompt gamma-ray spectra," *Nucl. Instrum. Methods Phys. Res. Sect. A Accel., Spectrom., Detect. Assoc. Equip.*, vol. 1046, Jan. 2023, Art. no. 167659. [Online]. Available: https://www.sciencedirect.com/science/article/pii/S0168900222009512

[10] P. Dendooven et al., "Short-lived positron emitters in beam-on PET imaging during proton therapy," *Phys. Med. Biol.*, vol. 60, no. 23, pp. 8923–8947, Dec. 2015. [Online]. Available: https://dx.doi.org/10.1088/0031-9155/60/23/8923

[11] A. Knopf, K. Parodi, T. Bortfeld, H. A. Shih, and H. Paganetti, "Systematic analysis of biological and physical limitations of proton beam range verification with offline PET/CT scans," *Phys. Med. Biol.*, vol. 54, no. 14, pp. 4477–4495, Jul. 2009. [Online]. Available: https://dx.doi.org/10.1088/0031-9155/54/14/008

[12] T. Werner et al., "Processing of prompt gamma-ray timing data for proton range measurements at a clinical beam delivery," *Phys. Med. Biology*, vol. 64, no. 10, May 2019, Art. no. 105023. [Online]. Available: https://dx.doi.org/10.1088/1361-6560/ab176d

[13] G. Ariño-Estrada et al., "Study of Čerenkov light emission in the semiconductors TlBr and TlCl for TOF-PET," *IEEE Trans. Radiat. Plasma Med. Sci.*, vol. 5, no. 5, pp. 630–637, Sep. 2021.

[14] "NIST element/compound/mixture selection," physics.nist.gov. Accessed: May 20, 2023. [Online]. Available: https://physics.nist.gov/PhysRefData/Xcom/html/xcom1.html

[15] "RefractiveIndex.infonk database," refractiveindex.info. Accessed: May 20, 2023. [Online]. Available: https://refractiveindex.info/

[16] F. Hueso-González et al., "Comparison of LSO and BGO block detectors for prompt gamma imaging in ion beam therapy," *J. Instrum.*, vol. 10, no. 9, Sep. 2015, Art. no. P09015. [Online]. Available: https://dx.doi.org/10.1088/1748-0221/10/09/P09015

[17] J. Krimmer, D. Dauvergne, J. Létang, and E. Testa, "Prompt-gamma monitoring in hadrontherapy: A review," *Nucl. Instrum. Methods Phys. Res. Sect. A Accel., Spectrom., Detect. Assoc. Equip.*, vol. 878, pp. 58–73, Jan. 2018. [Online]. Available: https://www.sciencedirect.com/science/article/pii/S0168900217308380

[18] S. Korpar, R. Dolenec, P. Križan, R. Pestotnik, and A. Stanovnik, "Study of TOF PET using Cherenkov light," *Nucl. Instrum. Methods Phys. Res. Sect. A Accel, Spectrom. Detect. Assoc. Equip.*, vol. 654, no. 1, pp. 532–538, Oct. 2011. [Online]. Available: https://www.sciencedirect.com/science/article/pii/S016890021101151X

[19] A. K. Biegun et al., "Time-of-flight neutron rejection to improve prompt gamma imaging for proton range verification: A simulation study," *Phys. Med. Biol.*, vol. 57, no. 20, pp. 6429–6444, Oct. 2012. [Online]. Available: https://dx.doi.org/10.1088/0031-9155/57/20/6429

[20] M. Jacquet et al., "A high sensitivity cherenkov detector for prompt gamma timing and time imaging," *Sci. Rep.*, vol. 13, no. 1, p. 3609, Mar. 2023. [Online]. Available: https://doi.org/10.1038/s41598-023-30712-x

[21] G. Terragni et al., "Time resolution studies of thallium based Cherenkov semiconductors," *Front. Phys.*, vol. 10, Mar. 2022, Art. no. 785627. [Online]. Available: https://www.frontiersin.org/articles/10.3389/fphy.2022.785627

[22] G. Ariño-Estrada et al., "First Cerenkov charge-induction (CCI) TlBr detector for TOF-PET and proton range verification," *Phys. Med. Biol.*, vol. 64, no. 17, p. 175001, Aug. 2019. [Online]. Available: https://dx.doi.org/10.1088/1361-6560/ab35c4

[23] G. Ariño-Estrada, H. Kim, J. Du, L. J. Cirignano, K. S. Shah, and S. R. Cherry, "Energy and electron drift time measurements in a pixel CCI TlBr detector with 1.3 MeV prompt-gammas," *Phys. Med. Biol.*, vol. 66, no. 4, Feb. 2021, Art. no. 044001. [Online]. Available: https://dx.doi.org/10.1088/1361-6560/abd419

[24] X. He, C. Trigila, G. Ariño-Estrada, and E. Roncali, "Potential of depth-of-interaction-based detection time correction in Cherenkov emitter crystals for TOF-PET," *IEEE Trans. Radiat. Plasma Med. Sci.*, vol. 7, no. 3, pp. 233–240, Mar. 2023.

[25] C. Trigila, G. Ariño-Estrada, S. I. Kwon, and E. Roncali, "The accuracy of Cerenkov photons simulation in Geant4/Gate depends on the parameterization of primary electron propagation," *Front. Phys.*, vol. 10, Apr. 2022, Art. no. 891602. [Online]. Available: https://www.frontiersin.org/articles/10.3389/fphy.2022.891602

[26] C. Trigila, E. Moghe, and E. Roncali, "Technical note: Standalone application to generate custom reflectance look-up table for advanced optical monte carlo simulation in GATE/Geant4," *Med. Phys.*, vol. 48, no. 6, pp. 2800–2808, 2021. [Online]. Available: https://aapm.onlinelibrary.wiley.com/doi/abs/10.1002/mp.14863

[27] H. Kim et al., "Thallium bromide gamma-ray spectrometers and pixel arrays," *Front. Phys.*, vol. 8, p. 55, Mar. 2020. [Online]. Available: https://www.frontiersin.org/articles/10.3389/fphy.2020.00055